J. Fluid Mech. (1989), *vol.* 207, *pp.* 393–418
Printed in Great Britain

Removing the irregular frequencies from integral equations in wave–body interactions

By C.-H. LEE AND P. D. SCLAVOUNOS
Department of Ocean Engineering, Massachusetts Institute of Technology, Cambridge, MA 02139, USA

(Received 22 June 1987 and in revised form 3 October 1988)

The paper presents a method that removes the effects of all irregular frequencies in boundary-integral equations governing the interaction of regular waves with floating bodies of general geometry. A modified integral equation is obtained by the linear superposition of the classical Green equation and its normal derivative with respect to the field point. The selection of a purely imaginary constant of proportionality ensures the removal of all irregular frequencies in the continuous problem and the appropriate selection of its magnitude eliminates their undesirable effects in its numerical implementation. Computations are presented of the added-mass and damping coefficients and exciting forces on a sphere and a truncated vertical cylinder, illustrating the effectiveness of the method.

1. Introduction

'Irregular' frequencies arise in boundary-integral formulations of wave problems, notably exterior problems in acoustics and surface-wave–body interactions. At the irregular frequencies the integral equations either possess no solutions, or if solutions exist they are not unique. The discrete approximation of these equations generates ill-conditioned linear systems for the unknown function on the body boundary and leads to appreciable errors. The existence of irregular frequencies is tied to the selection of the specific boundary-integral equation and in no way reflects an irregularity in the solution of the original boundary-value problem, which under mild restrictions on the body geometry accepts a unique solution at all frequencies.

The occurrence of irregular frequencies in boundary-integral equations arising in wave interactions with surface-piercing bodies is pointed out by John (1950). Their detrimental effects in applications did not become evident until the late sixties, when Frank (1967) developed a two-dimensional panel method for the prediction of the added-mass and damping coefficients of ship sections. Frank used the 'source distribution' method which leads to the solution of a Fredholm integral equation of the second kind for the source strength over the body boundary. His numerical results displayed a substantial error in the predictions of the added-mass and damping coefficients near the irregular frequencies. Subsequent numerical studies confirmed the presence of the irregular-frequency error in two- and three-dimensional problems, both in connection with the source distribution and the 'Green' methods. The latter is based on the application of Green's theorem which leads to the solution of a Fredholm integral equation of the second kind for the velocity potential on the body boundary.

The kernel in the Green integral equation is the transpose of the kernel in the source-distribution method. The irregular frequencies of the two equations are the same because they coincide with the zeros of their common Fredholm determinant.

They can be shown to coincide with the eigenfrequencies of the interior Dirichlet problem (Ohmatsu 1975), thus forming an infinite discrete set. In the vicinity of the irregular frequencies the properties of the source strength and velocity potential are quite different. The source-distribution integral equation has no solution 'at' the irregular frequencies, and the source strength can be shown to possess a principal-value singularity in their vicinity. This singular behaviour is not present in the velocity potential defined either as a distribution of wave sources over the body boundary or obtained from the solution of the Green integral equation. Unlike its source-distribution counterpart the Green equation can be shown to possess a non-unique solution at the irregular frequencies, by virtue of Fredholm's third theorem. Adachi & Ohmatsu (1979) show that its right-hand side is orthogonal to the eigensolutions of its transpose, the source-distribution equation.

In spite of the non-singular behaviour of the velocity potential near the irregular frequencies, the condition number of both the source distribution and the Green equation is large in their vicinity. Discretization errors in their numerical solution by panel methods translate into large errors in the solution over a substantial frequency band around the irregular frequencies. The width of this 'polluted' frequency band can be reduced by increasing the number of panels. In practice this treatment is unacceptable because it entails a substantial increase in the computational effort. Ohmatsu (1975) suggested the addition of a rigid lid on the body waterplane area. Its presence eliminates the 'resonance' associated with the interior Dirichlet eigen-problem and therefore eliminates the effects of the irregular frequencies. This method is effective with both the source and the Green methods in two and three dimensions, at the cost of using additional panels on the body waterplane area. Ogilvie & Shin (1978) removed the first irregular frequency in two dimensions by placing a point wave source on the interior free surface acting as an absorber of the energy of the corresponding resonant Dirichlet eigensolution. Ursell (1981) showed that the use of a sequence of singularities is necessary for the removal of more than the first irregular frequency from the integral equation. Sayer (1980) extended this technique in water of finite depth and Wu & Price (1987) for the case of twin bodies.

Partly as a result of the inherent presence of irregular frequencies in boundary-integral equations based on the wave Green function, a new class of hybrid methods of solution surfaced. Yeung (1973) utilized an integral representation of the flow near the body, based on the Rankine source $1/r$ and a distribution of panels over the body boundary, free surface and a matching boundary. In the domain exterior to this boundary a series representation was used. In water of infinite depth in two dimensions this technique was further developed by Nestegard & Sclavounos (1984). A proof that this formulation is free of irregular frequencies was given by Angell, Hsiao & Kleinman (1983). An alternative hybrid method based on a finite-element representation of the flow in the interior domain was studied by Bai & Yeung (1974). In three dimensions this method is reviewed by Mei (1978). Of different flavour is the approach by Martin (1981) in two and three dimensions, based on the null-field equation method and exercised for bodies of mathematical shape. In all these methods irregular-frequency effects were found not to occur.

In related work in acoustic radiation and scattering, Leis (1965), Brakhage & Werner (1965), and Panich (1965) independently proposed the removal of the irregular frequencies in the source-distribution method by supplementing the single-layer potential by a distribution of normal dipoles with moment proportional to the source strength. By selecting the coupling constant to be complex they generated a modified integral equation free of irregular frequencies. In an acoustic scattering

problem, Burton & Miller (1971) obtained a similar equation by the linear superposition of the Green integral equation and its normal derivative with respect to the field point. The analytical properties of these modified equations in acoustics are studied by Colton & Kress (1983) and in surface-wave body interactions by Kleinman (1982). A variational form of this modified integral formulation, coupled to a finite-element layer surrounding the body boundary, was studied by Euvrard *et al.* (1981) for the computation of the interaction of surface waves with floating bodies.

It is the objective of the present study to demonstrate the effectiveness of this modified integral formulation in removing the irregular frequency effects in surface-wave–body interactions, applied directly over the body boundary and requiring no prior regularization of the integral operator. In both the radiation and diffraction problems, the linear superposition of the Green equation and its normal derivative is solved for the respective potentials. Their numerical solution is implemented in a radiation/diffraction panel code and all irregular frequencies are removed. The increase in the computational effort is not substantial relative to the effort required for the solution of the Green equation. The implementation of the present method utilizes the same number of panels and unknowns as in the Green equation and requires the evaluation of the second derivatives of the wave source potential. In deep water they can be related to lower-order derivatives by recurrence relations, and in finite depth they can be obtained at a small additional computational cost.

The Green equation for the velocity potential is Fredholm of the second kind, while its normal derivative is a principal-value type equation of the first kind with poor conditioning. The singularity in the kernel of the latter equation is similar to that in the lifting-surface equation for the distribution of vorticity in thin-wing theory. Each equation independently solves the radiation and diffraction boundary-value problems, therefore their linear combination does as well. The irregular frequencies of the Green equation coincide with the eigenfrequencies of the interior Dirichlet problem, and those of its normal derivative with the eigenfrequencies of the interior Neumann problem. Their linear combination has irregular frequencies, unless the coupling constant is complex. Numerical experiments suggested that a positive purely imaginary coupling constant generates the best results. The proper selection of its magnitude is essential for the successful numerical implementation of the method. It is shown that an optimal value exists, and is determined by minimizing the condition number of the modified integral equation at the first irregular frequency of the Green equation. Similar studies have been conducted in acoustic and electromagnetic scattering by Kress (1983) and for an exterior Stokes flow by Hsiao & Kress (1985).

The performance of the method is illustrated by the computation of the added-mass and damping coefficients and exciting forces on a sphere and a truncated vertical cylinder. The errors in the vicinity of all Dirichlet and Neumann irregular frequencies are removed, leaving the quality of the numerical predictions away from their location unaffected.

2. Formulation

Regular plane progressive waves interact with a floating body which undergoes small-amplitude oscillations around a stationary position. The flow is assumed to be irrotational, and the free-surface and body-boundary conditions are linearized. A time-harmonic dependence applies throughout, permitting the use of complex

velocity potentials to describe the incident, radiation and diffraction wave disturbances. The real part of the product of all complex quantities with the factor $e^{i\omega t}$ is understood hereafter. Because of the association of irregular frequencies with the interior Dirichlet problem, their effects in water of finite or infinite depth are the same. Therefore, only the last case is studied here. The incident wave potential is defined by

$$\varphi_0 = \frac{igA}{\omega} e^{\nu z - i\nu x \cos\beta - i\nu y \sin\beta}, \tag{2.1}$$

where A is the wave amplitude, ω its frequency, $\nu = \omega^2/g$ and β the propagation angle of the incident waves relative to the positive x-axis. The Cartesian coordinate system (x, y, z), illustrated in figure 1, is fixed relative to the $z = 0$ plane.

Linearity allows the decomposition of the body-generated wave disturbance into the radiation component φ_R and the diffraction component φ_7, with

$$\varphi_R = i\omega \sum_{j=1}^{6} \xi_j \varphi_j, \tag{2.2}$$

where ξ_j, $j = 1, \ldots, 6$ are the complex amplitudes of the oscillatory body displacement in its six rigid-body degrees of freedom. The complex velocity potentials φ_j, $j = 1, \ldots, 7$ satisfy the Laplace equation in the fluid domain, are subject to the free-surface condition

$$\varphi_{jz} - \nu\varphi_j = 0 \tag{2.3}$$

on the $z = 0$ plane, the Sommerfeld radiation condition at infinity, and on the body boundary they satisfy the conditions

$$\varphi_{jn} = n_j, \quad j = 1, \ldots, 6, \tag{2.4}$$

$$\varphi_{7n} = -\varphi_{0n}, \tag{2.5}$$

where n_i, $i = 1, 2, 3$ are the Cartesian components of a unit vector, normal to the body surface and pointing out of the fluid domain, and $(n_4, n_5, n_6) = (x, y, z) \times (n_1, n_2, n_3)$.

The radiation and diffraction velocity potentials will be determined by applying Green's theorem, utilizing as the Green function the wave source potential

$$G(x;\xi) = \frac{1}{r} + \frac{\nu}{2\pi} \int_0^\infty dk \int_0^{2\pi} d\vartheta \frac{k+\nu}{k-\nu} e^{k(z+\zeta) + ik(x-\xi)\cos\theta + ik(y-\eta)\sin\theta}, \tag{2.6}$$

$$r^2 = (x-\xi)^2 + (y-n)^2 + (z-\zeta)^2 \tag{2.7}$$

due to a point source located at the point (ξ, η, ζ), which satisfies the Laplace equation and free-surface conditions. The contour integral over the positive k-axis is indented over the pole in order to ensure the satisfaction of the Sommerfeld radiation condition. The derivation of (2.6) is detailed in Wehausen & Laitone (1960). For the radiation potentials φ_j, Green's theorem yields the following Fredholm integral equation over the body boundary:

$$2\pi\varphi_j(x) + \iint_{S_b} d\xi \varphi_j(\xi) \frac{\partial G(\xi; x)}{\partial n_\xi} = \iint_{S_b} d\xi n_j(\xi) G(\xi : x). \tag{2.8}$$

It is hereafter understood that the x, ξ variables appearing in (2.8) and all ensuing integral equations denote vectorial positions. An integral equation similar to (2.8) can be obtained for the diffraction velocity potential φ_7 by replacing n_j by $-\partial\varphi_0/\partial n$ in the right-hand side of (2.8). An alternative, and somewhat more attractive,

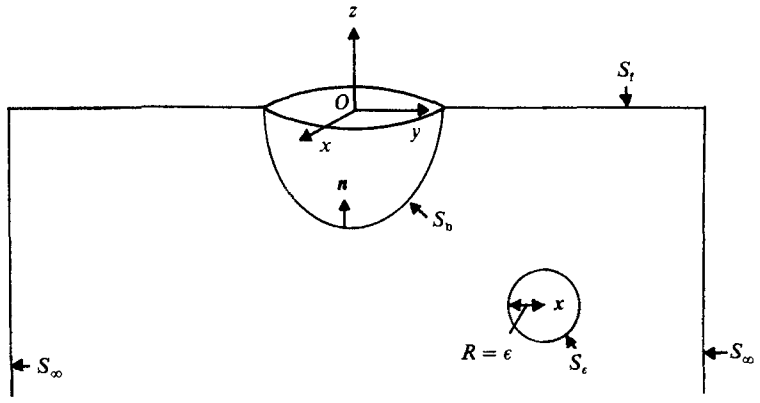

FIGURE 1. The Cartesian coordinate system.

integral equation exists for the sum of the incident and diffraction potentials φ_D. It is

$$2\pi\varphi_D(x)+\iint_{S_b} d\xi\varphi_D(\xi)\frac{\partial G(\xi;x)}{\partial n_\xi}=4\pi\varphi_0(x). \tag{2.9}$$

Its derivation parallels that in analogous aerodynamic flows where the incident flow is potential flow (Moran 1984). Other than the pointwise distribution of the radiation and diffraction velocity potentials, of interest in applications are the added-mass and damping coefficients, a_{ij} and b_{ij} respectively. They are related to the real and imaginary parts of the complex impedance force or moment in the ith direction due to the forced oscillation of the body in the jth direction. They are defined as follows

$$a_{ij}-(i/\omega)\,b_{ij}=\rho\iint_{S_b} n_i\varphi_j\,ds. \tag{2.10}$$

The corresponding wave-exciting forces and moments in the ith direction are obtained from the solution of the diffraction problem, and are defined by the expression

$$X_i=-i\omega\rho\iint_{S_b}\varphi_D\,n_i\,ds. \tag{2.11}$$

Section 3 shows that (2.8) and (2.9) possess non-unique solutions at the eigen-frequencies of the interior Dirichlet problem, and presents the method that removes them. Computations of the added-mass and damping coefficients and exciting force are presented in §4.

3. Irregular frequencies and their removal

This section reviews aspects of the theory on the occurrence of the irregular frequencies in the classical Green integral equation and their removal in its modified form.

The integral equations (2.8) and (2.9) differ only in their right-hand sides. Therefore, should homogeneous solutions exist, they are common and occur at the same frequencies. Denote by

$$\psi(x)=\iint_{S_b} d\xi\varphi(\xi)\frac{\partial G(x;\xi)}{\partial n_\xi} \tag{3.1}$$

the velocity potential $\psi(x)$ at the field point x inside the body, due to a distribution of normal dipoles on the body boundary with moment equal to $\varphi(\xi)$. As the field point x approaches the interior of the body boundary, the velocity potential ψ takes the limiting value

$$\psi(x) = 2\pi\varphi(x) + \iint_{S_b} d\xi \varphi(\xi) \frac{\partial G(x;\xi)}{\partial n_\xi}. \tag{3.2}$$

If $\psi(x) = 0$ on the interior of the body boundary, the existence of homogeneous solutions to (2.8) and (2.9) is equivalent to the existence of a non-trivial 'dipole moment' $\varphi(\xi)$ defining, via (3.1), a non-vanishing velocity potential ψ inside the body. A non-trivial velocity potential ψ in the body interior, subject to $\psi = 0$ on its interior boundary and the free-surface condition (2.3) on $z = 0$, exists at the eigenfrequencies of the interior Dirichlet problem. They form an infinite discrete set, and are hereafter named *Dirichlet frequencies*.

The integral equations (2.8) and (2.9) are not the only possible equations solving the radiation and diffraction problems. Since properties of the interior domain define the existence and the location of the irregular frequency, we may reason backwards in search of an integral equation free of homogeneous solutions. What interior boundary condition for the velocity potential ψ leads to trivial interior solutions at all frequencies? Burton & Miller (1971) suggest a linear combination of the Dirichlet and Neumann boundary conditions which leads to an interior eigenproblem accepting trivial solutions at all frequencies. Let ψ be subject to

$$\psi + \alpha \frac{\partial \psi}{\partial n} = 0 \tag{3.3}$$

on the interior boundary, where α is a complex constant. Combining (3.1) and (3.3), the dipole moment $\varphi(\xi)$ is subject to

$$0 = 2\pi\varphi(x) + \iint_{S_b} d\xi \varphi(\xi) \frac{\partial G(x;\xi)}{\partial n_\xi} + \alpha \frac{\partial}{\partial n_x} \iint_{S_b} d\xi \varphi(\xi) \frac{\partial G(x;\xi)}{\partial n_\xi}. \tag{3.4}$$

The homogeneous equation (3.4) accepts only the trivial solution if the imaginary part of α is non-zero. Following Kleinman (1982), we apply Green's theorem to ψ and its complex conjugate ψ^*, use the free surface and the interior condition (3.3) to obtain

$$\iiint_V |\nabla\psi|^2 \, dv = \iint_{S_b+S_f} ds \, \psi \frac{\partial \psi^*}{\partial n} = \nu \iint_{S_f} ds \, |\psi|^2 + \alpha \iint_{S_b} ds \left| \frac{\partial \psi}{\partial n} \right|^2 \tag{3.5}$$

Taking the imaginary part of both sides of (3.5), we conclude that for a non-vanishing imaginary part of the complex constant α, $\partial\psi/\partial n = 0$ on the interior boundary. Combining this condition with (3.3) it follows that $\psi = 0$ as well. Interior eigensolutions subject to the former condition occur at the Neumann frequencies and those subject to the latter occur at the Dirichlet frequencies. Frequencies from one set may coalesce with frequencies from the other for certain body geometries. This is illustrated later in the section for a truncated vertical cylinder. The existence, however, of non-trivial interior eigensolutions subject simultaneously to the homogeneous Dirichlet and Neumann conditions on the interior boundary demands the coalescence of the corresponding mode shapes as well, which is not the case. This follows from Green's representation theorem which ensures that $\psi \equiv 0$ in the interior domain when both $\psi = 0$ and $\partial\psi/\partial n = 0$ hold on its boundary. Therefore, the coalescence of the Dirichlet and Neumann frequencies is expected not to be

responsible for any ill-conditioning in the matrix equation or generate a substantial error of the numerical solution in their vicinity. Supporting numerical evidence is presented in the next section.

The coalescence of Dirichlet and Neumann frequencies is next shown for a truncated vertical circular cylinder with draught T and radius R. Eigensolutions of the interior Dirichlet problem take the form

$$\begin{Bmatrix} \psi^{\mathrm{D}}_{C,m} \\ \psi^{\mathrm{D}}_{S,m} \end{Bmatrix} = \sinh k(z+T) \begin{Bmatrix} \cos m\theta \\ \sin m\theta \end{Bmatrix} J_m(kr), \tag{3.6}$$

where $J_m(x)$ are the Bessel functions of order m. The wavenumber k is determined from the Dirichlet condition on $r = R$,

$$J_m(k_s R) = 0, \quad s = 1, \ldots. \tag{3.7}$$

The Dirichlet frequencies corresponding to the modes defined by (3.6) and (3.7) are determined by enforcing the free-surface condition (2.3), and in non-dimensional form are defined by the relationship

$$\nu^{\mathrm{D}}_{m,s} R = \frac{\omega^2_{m,s} R}{g} = k_{m,s} R \coth k_{m,s} R \left(\frac{T}{R}\right). \tag{3.8}$$

The corresponding eigensolutions of the interior Neumann problem are

$$\begin{Bmatrix} \psi^{\mathrm{N}}_{C,n} \\ \psi^{\mathrm{N}}_{S,n} \end{Bmatrix} = \cosh k(z+T) \begin{Bmatrix} \cos n\theta \\ \sin n\theta \end{Bmatrix} J_n(kr), \tag{3.9}$$

$$J'_n(k_s R) = 0, \quad s = 1, \ldots, \tag{3.10}$$

$$\nu^{\mathrm{N}}_{n,s} R = \frac{\omega^2_{n,s} R}{g} = k_{n,s} R \tanh k_{n,s} R \left(\frac{T}{R}\right). \tag{3.11}$$

Denote the roots of $J_n(x)$ by $j_{n,s}, s = 1, \ldots$ and of $J'_n(x)$ by $j'_{n,s}, s = 1, \ldots$. The coalescence of Dirichlet and Neumann frequencies is equivalent to the equality of the two functions of the parameter $\delta = T/R$:

$$j_{m,s} \coth j_{m,s}\delta = j'_{n,t} \tanh j'_{n,t}\delta, \tag{3.12}$$

where $j_{m,s}, j'_{n,t}$ are fixed roots of Bessel functions. The function on the left-hand side is monotonically decreasing, with an asymptotic behaviour $1/\delta$ as $\delta \to 0$ and tending to $j_{m,s}$ as δ tends to infinity. The function on the right-hand side is monotonically increasing from zero to $j'_{n,t}$ as δ tends to infinity. Therefore, values of δ that solve (3.12) exist if the following inequality is satisfied:

$$j_{m,s} < j'_{n,t}. \tag{3.13}$$

Three solutions of (3.12) subject to (3.13) are, for example, $\delta = 0.367$, $\nu R = 3.398$ for $m = n = 0$, $s = 1$, $t = 2$, and $\delta = 0.527$, $\nu R = 2.82$ for $s = t = 1$, $m = 0$, $n = 2$ and $\delta = 0.455$, $\nu R = 5.23$ for $s = t = 1$, $m = 0$, $n = 4$. It is clear from this analysis that the coalescence of Dirichlet and Neumann frequencies is not accompanied by the equality of their corresponding eigenmodes.

The right-hand sides for the radiation and diffraction problems, corresponding to (3.4), are obtained as follows. Using Green's identity, the radiation potentials in the fluid domain are defined by

$$4\pi\varphi_j(x) + \iint_{S_b} \mathrm{d}\xi \varphi_j(\xi) \frac{\partial G(\xi; x)}{\partial n_\xi} = \iint_{S_b} \mathrm{d}\xi n_j(\xi) G(\xi; x). \tag{3.14}$$

The normal derivative of (3.14) is evaluated by taking the inner product of its gradient with respect to the field point x with the normal vector $\boldsymbol{n}$. The result is

$$\frac{\partial}{\partial n_x}\iint_{S_b} d\xi \varphi_j(\xi)\frac{\partial G(\xi;x)}{\partial n_\xi} = -2\pi n_j(x) + \iint_{S_b} d\xi\, n_j(\xi)\frac{\partial G(\xi;x)}{\partial n_x}, \tag{3.15}$$

which is an integral equation of the first kind for the velocity potential φ_j. Compared to (2.8), it is less attractive for computation because of its poor conditioning and the need to interpret and evaluate carefully the double-normal derivative of the Green function. Its irregular frequencies coincide with the Neumann frequencies, as can be seen by comparing the left-hand side of (3.15) with the normal derivative of the right-hand side of (3.1). The linear combination of (2.8) and (3.15) leads to the desired modified equation for the radiation velocity potentials φ_j:

$$2\pi\varphi_j(x) + \iint_{S_b} d\xi \varphi_j(\xi)\frac{\partial G(\xi;x)}{\partial n_\xi} + \alpha\frac{\partial}{\partial n_x}\iint_{S_b} d\xi \varphi_j(\xi)\frac{\partial G(\xi;x)}{\partial n_\xi}$$
$$= \iint_{S_b} d\xi\, n_j(\xi)\, G(\xi;x) - 2\pi\alpha n_j(x) + \alpha\iint_{S_b} d\xi\, n_j(\xi)\frac{\partial G(\xi;x)}{\partial n_x}, \tag{3.16}$$

which is the same equation as that derived and studied by Kleinman (1982). For the sum of the incident and diffraction potentials, the corresponding equation takes the form

$$2\pi\varphi_D(x) + \iint_{S_b} d\xi \varphi_D(\xi)\frac{\partial G(\xi;x)}{\partial n_\xi} + \alpha\frac{\partial}{\partial n_x}\iint_{S_b} d\xi \varphi_D(\xi)\frac{\partial G(\xi;x)}{\partial n_\xi}$$
$$= 4\pi\left[\varphi_0(x) + \alpha\frac{\partial\varphi_0(x)}{\partial n_x}\right]. \tag{3.17}$$

The homogeneous operator of both equations is identical to (3.4) which was shown to possess only the trivial solution, thus confirming that (3.16) and (3.17) are free of Dirichlet or Neumann irregular frequencies.

Colton & Kress (1983) point out that in the numerical procedure one can directly descretize (3.16) and (3.17) or use the regularized form obtained by a pre-multiplication of these equations by a frequency-independent operator. With this operation the unbounded operator involving the double normal derivative of the Green function (2.6) can be rendered bounded. This operation is equivalent to an integration by parts and it reduced the strength of the singularity in the double normal derivative. Burton & Miller (1971) suggest the same regularization process. The disadvantage of this process is that it entails the set-up and premultiplication of the modified equation by a matrix. In the light of the substantial increase in the computational effort associated with such a process for a large number of panels, we attempted the direct numerical solution which is described in the next section.

4. Numerical solution

The numerical solution of (3.16) and (3.17) was carried out by a panel method. The body wetted surface is fitted with a large number of plane quadrilaterals, the velocity potential is assumed piecewise constant over their surface and the integral equation

is solved by collocation at the panel centroids. These steps reduce the continuous equation (3.16) to a matrix equation for the velocity potentials φ_i,

$$2\pi\varphi_i + \sum_{j=1}^{N} \varphi_j \iint_{S_j} \mathrm{d}\xi \frac{\partial G(\xi; x_i)}{\partial n_\xi} + \alpha \sum_{j=1}^{N} \varphi_j \frac{\partial}{\partial n_{x_i}} \iint_{S_j} \mathrm{d}\xi \frac{\partial G(\xi; x_i)}{\partial n_\xi}$$
$$= \sum_{j=1}^{N} n_j \iint_{S_j} \mathrm{d}\xi\, G(\xi; x_i) - 2\pi\alpha n_i + \alpha \sum_{j=1}^{N} n_j \iint_{S_j} \mathrm{d}\xi \frac{\partial G(\xi; x_i)}{\partial n_{x_i}}, \quad (4.1)$$

where $i = 1, \ldots, N$ and x_i are the vector coordinates of the centroid of the ith panel. Here the subscripts i, j are panel rather than mode-of-motion indices, S_j denotes the area of the jth panel and N is the total number of panels. The discrete form of the diffraction integral equation (3.17) is similar to (4.1).

If $\alpha = 0$, (4.1) reduces to the discrete form of the Green equation, the solution of which has been found to generate large errors in the vicinity of the irregular frequencies. In connection with the panel code used in the present study, their detrimental effects are illustrated in two dimensions in Sclavounos & Lee (1985) and in three dimensions in Breit, Newman & Sclavounos (1985).

The inclusion of the irregular-frequency correction in (4.1) for $\alpha \neq 0$ requires the interpretation and evaluation of the double normal derivative of the Green function in the left-hand side. For $i \neq j$, this normal derivative is non-singular and the normal derivative with respect to the x_i coordinate and the integration over S_j can be interchanged. When $i = j$, it follows that the double normal derivative of the Green function G in (4.1) is equal to the normal velocity induced at the centroid of the jth panel by a layer of normal dipoles of constant moment φ_j distributed over its surface. This normal velocity is known to exist (cf. Kellog 1929) and can be evaluated by interchanging the normal-derivative operation with the integration and interpreting the singularity in the resulting double normal derivative under the integral sign in the principal value sense. Moreover, it can be shown that this singularity is identical to that encountered in lifting-surface theory.

Define a local Cartesian coordinate system centred at the centroid of the jth panel with the ζ_l axis normal to the plane of the panel and pointing in the direction of the normal vector $\boldsymbol{n}$, and the ξ_l, η_l axes lying on the panel surface. Replacing the Green function G by its singular component $1/r = 1/|\boldsymbol{x}_l - \boldsymbol{\xi}_l|$, it follows that

$$D_j = \frac{\partial}{\partial n_{x_l}} \iint_{S_j} \mathrm{d}\xi_l\, \mathrm{d}\eta_l \frac{\partial(1/r)}{\partial n_{\xi_l}} = -\iint_{S_j} \mathrm{d}\xi_l\, \mathrm{d}\eta_l \frac{\partial^2(1/r)}{\partial \zeta_l^2}. \quad (4.2)$$

Invoking the Laplace equation and a known Green identity, we obtain

$$D_j = \iint_{S_j} \mathrm{d}\xi_l\, \mathrm{d}\eta_l \left(\frac{\partial^2}{\partial \xi_l^2} + \frac{d^2}{\partial \eta_l^2}\right)\left(\frac{1}{r}\right) = \int_{C_j} \mathrm{d}l \frac{\partial(1/r)}{\partial s_{\xi_l}}, \quad (4.3)$$

where C_j is the contour of the jth quadrilateral and $\boldsymbol{s}$ is the unit outwards normal vector on this contour lying on the plane of the panel (figure 2).

Denoting by $\boldsymbol{t}$ the unit tangent vector on C_j, and using the identity $\boldsymbol{s} = \boldsymbol{n} \times \boldsymbol{t}$ it follows that

$$D_j = \boldsymbol{n} \cdot \int_{C_j} \mathrm{d}l[\boldsymbol{t} \times \nabla_{\xi_l}(1/r)] = -\boldsymbol{n} \cdot \int_{C_j} \mathrm{d}\boldsymbol{l} \times \nabla_{x_j}(1/r) \quad (4.4)$$

which reduces D_j to an application of the Biot–Savart law, providing the normal velocity at the panel centroid $\boldsymbol{x}_j$ induced by a vortex filament over the panel contour.

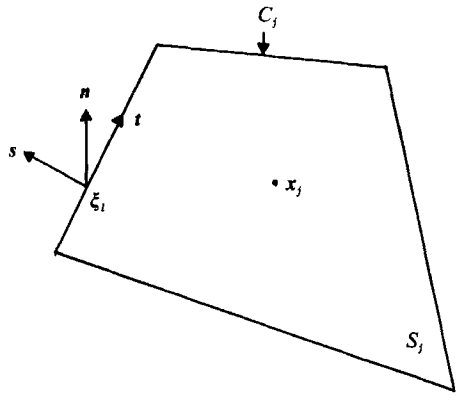

FIGURE 2. Definition sketch for the local coordinate system.

Equation (4.4), derived here for $i = j$, forms the basis of the vortex-lattice method used for the solution of lifting-surface equations. It can be shown that (4.4) can be expressed in closed form in terms of elementary transcendental functions by combining the contributions from the four straight segments that C_j consists of. A generalization of (4.4) for $i \neq j$ follows similar steps.

Summarizing, all elements in the matrix equation (4.1) have been evaluated by subtracting the singular component $1/r$ from G and integrating it analytically over the panels using the formulae of Hess & Smith (1966) and Newman (1986), including (4.4) for the terms involving the double normal derivative of $1/r$. The regular part of G and its spatial derivatives were integrated using a single-node numerical quadrature centred at the panel centroid. For pairs of panels (i,j) sufficiently distant from each other, the analytical treatment of the Rankine singularity $1/r$ is unnecessary. For these elements, the entire Green function and its spatial derivatives are integrated over the panels by the single-node quadrature formula.

The selection of the panel centroids as the collocation points is essential for the proper numerical convergence of the present scheme. This is due to the presence of the double normal derivative in the first-kind component in the matrix equation (4.1), which is seen from (4.4) to generate infinite influence coefficients if the collocation point is allowed to approach the panel sides. A similar property is shared by vortex lattice methods where convergence is ensured by selecting the collocation point to lie at the panel centroid or in its near vicinity. In spite of such a selection, the numerical conditioning of the first-kind component in (4.1) is poor relative to its second-kind counterpart. It is the objective of the present study to show that by a proper selection of the coupling constant α the quality of the final results is not affected, while at the same time the irregular-frequency errors are removed.

The selection of the 'proper' value for α was carried out by minimizing the condition number κ of the modified equation, or equivalently by maximizing its inverse $\lambda = 1/\kappa$ which will be the quantity considered hereafter. The mathematical library LINPACK was used to determine κ. It was found by numerical experimentation with alternative methods that the estimate provided by LINPACK is both an inexpensive and reliable indicator of the numerical conditioning of the associated matrix. The value of λ depends on the wave frequency and the complex parameter α. The maximization of λ over a wide range of frequencies is expensive and turns out to be unnecessary. It is more appropriate to study its behaviour in the vicinity of the Dirichlet or Neumann frequencies of the second- or first-kind

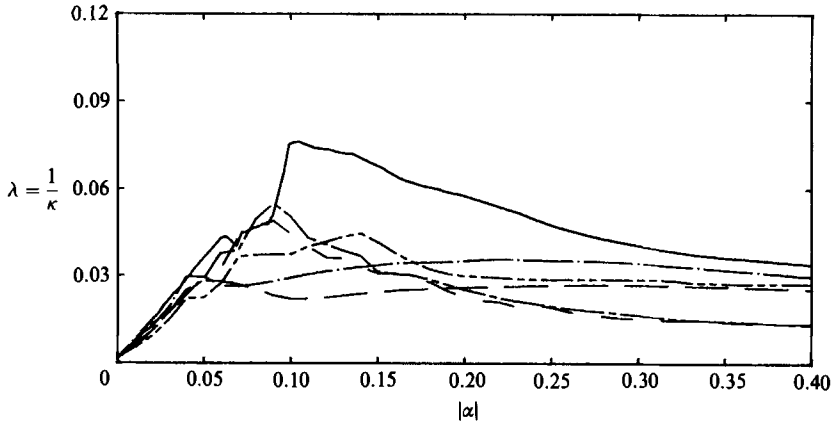

FIGURE 3. Inverse of the condition number with different phase of α for the sphere oscillating in heave at the first Dirichlet irregular frequency, as a function of $|\alpha|$: — – —, 45°; ——, 90°; —·—, 135°; — —, 225°; —··—, 270°; — — —, 315°.

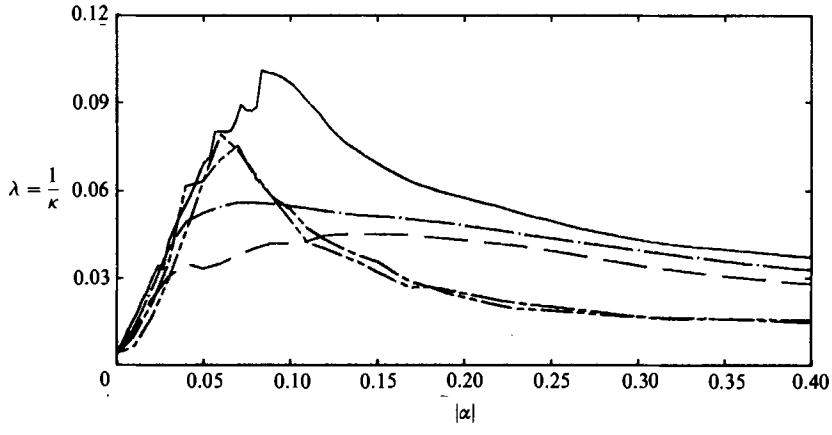

FIGURE 4. As figure 3, but for the sphere oscillating in sway.

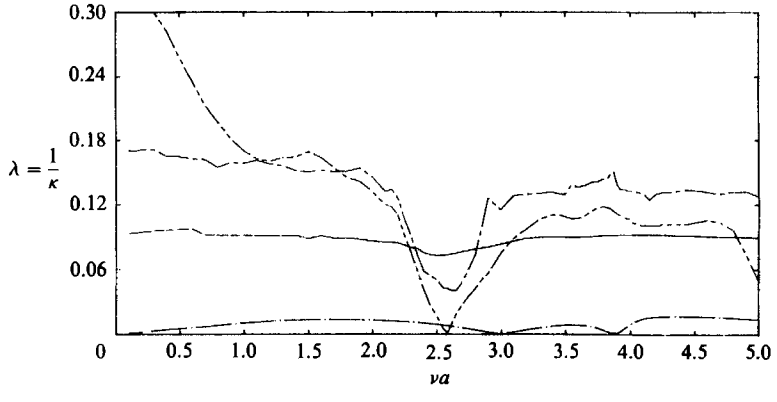

FIGURE 5. Inverse of the condition number λ of (4.1) for the sphere oscillating in heave, as a function of the non-dimensional wavenumber νa where a is the sphere radius: — – – —, $\beta = 0$; — – —, $\beta = 0.06$; ——, $\beta = 0.11$; —·—, $\beta = \infty$.

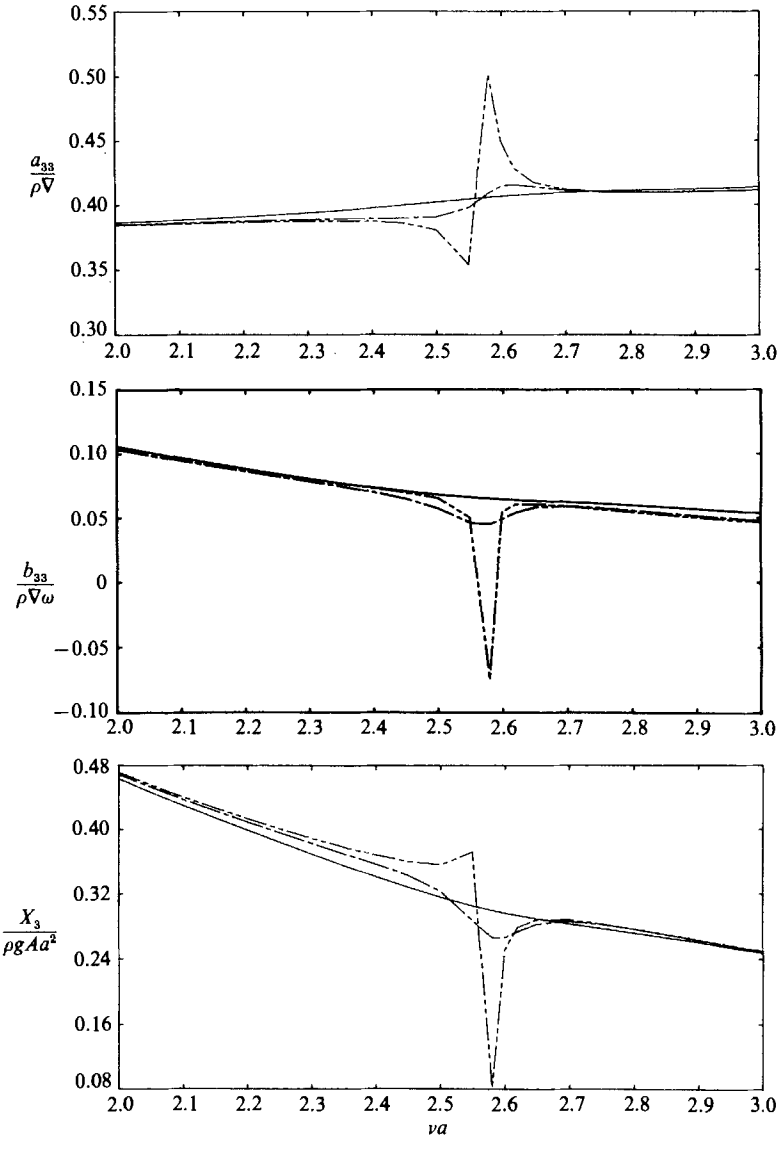

FIGURE 6. Heave added-mass and damping coefficients and modulus of the exciting force on the sphere near the first Dirichlet irregular frequency, as functions of νa. They are non-dimensionalized by a, the displacement ∇, the water density ρ, the frequency ω, the acceleration due to gravity g and the incident-wave amplitude A: — — — —, $\beta = 0$; — — —, $\beta = 0.02$; ——, $\beta = 0.11$.

components of (4.1). The first Dirichlet frequency was selected to be the frequency at which the maximisation of λ was carried out by varying α. Numerical evidence will be presented supporting the conclusion that this choice produces very good results near the other Dirichlet and Neumann frequencies and more generally over the entire frequency range of practical interest.

The selection of the modulus and phase of α that maximizes λ at the first Dirichlet frequency was carried out by studying the variation of λ as a function of the modulus of α with phase set equal to 45°, 90°, 135°, 225°, 270° and 315°. The corresponding curves are illustrated in figures 3 and 4 for a sphere oscillating in heave and sway

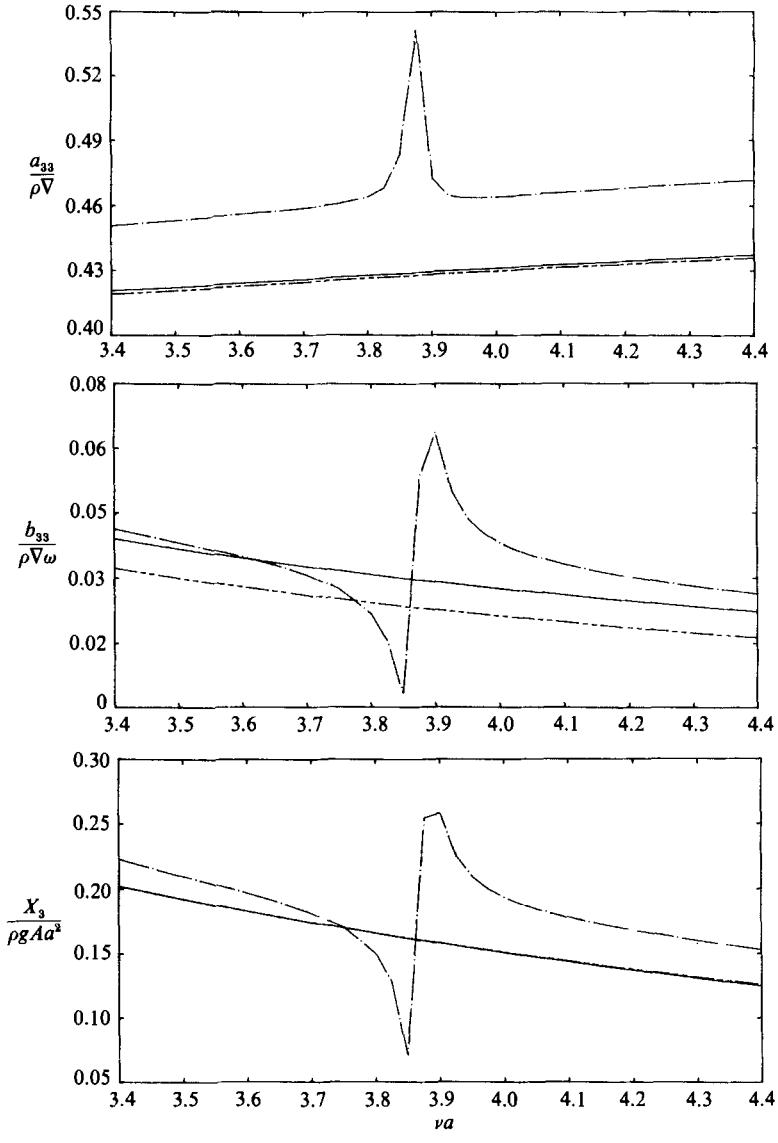

FIGURE 7. Heave added-mass and damping coefficients and modulus of the exciting force on the sphere near the second Neumann irregular frequency, as functions of νa: — — —, $\beta = 0$; ——, $\beta = 0.11$; —·—, $\beta = \infty$.

respectively. These results produce two essential pieces of information regarding the optimal modulus and phase of α. It is evident that over most of $|\alpha|$ the choice of its phase being equal to 90° leads to larger values for λ. More importantly, the largest value of λ is attained for the same phase and for $|\alpha| \approx 0.1$, both for heave and sway. We may therefore conclude that for the sphere, the optimal value of the complex coupling parameter is $\alpha \approx 0 + 0.1\mathrm{i}$. It may be noticed that λ tends to a small value at $|\alpha| = 0$, signifying that the numerical conditioning of the unmodified equation is poor at the first Dirichlet frequency, as expected.

Recall that the determination of the optimal value for α was carried out at the first Dirichlet frequency. The determination of that frequency in practice for the sphere

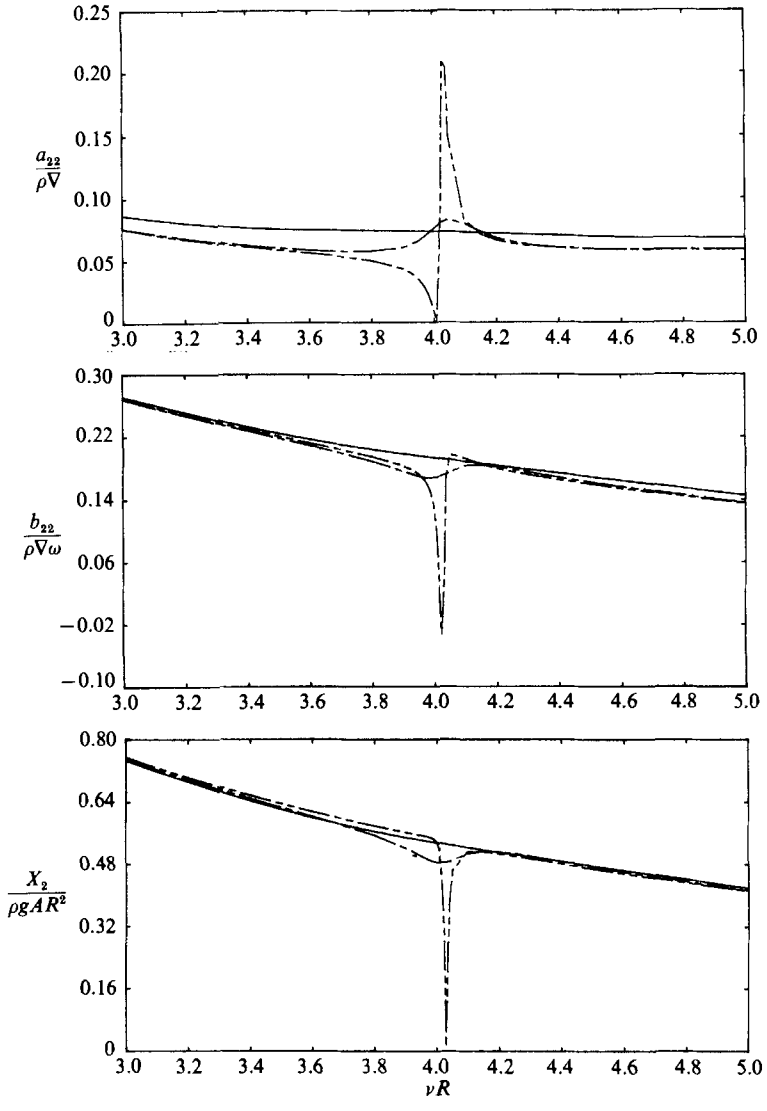

FIGURE 8. Sway added-mass and damping coefficients and modulus of the exciting force on the cylinder near the first Dirichlet irregular frequency, as functions of νR where R is the cylinder radius: — — —, $\beta = 0$; — — —, $\beta = 0.02$; ——, $\beta = 0.15$.

and more general bodies will become clear shortly. The variation of λ over a wide frequency range is shown in figure 5 for the sphere oscillating in heave. The remaining curves illustrate the variation of λ for other 'non-optimal' values of $\beta = |\alpha|$. The curve corresponding to $\beta = \infty$ represents the result when only the first-kind component of (4.1) is accounted for.

It is instructive here to make certain observations, noting that all values of β correspond to a 90° phase angle, or $\alpha = \mathrm{i}\beta$. For $\beta = 0$, i.e. for the Green equation, λ vanishes at the first Dirichlet frequency. For $\beta = \infty$, i.e. for the first-kind equation, λ vanishes at three frequencies which correspond to the first three Neumann frequencies. For $\beta_{\mathrm{opt}} = 0.11$, λ attains a nearly constant value which persists even at higher frequencies. This value is smaller than the corresponding value for the Green

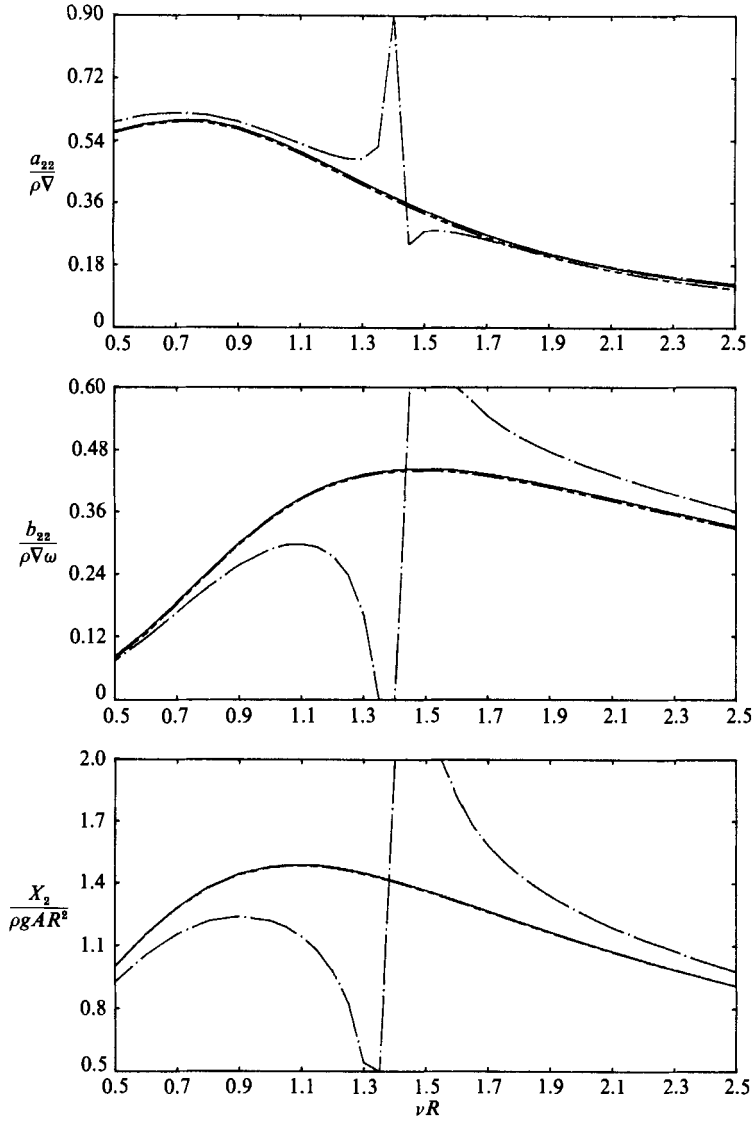

FIGURE 9. Sway added-mass and damping coefficients and modulus of the exciting force on the sphere near the first Neumann irregular frequency, as functions of νR: — — —, $\beta = 0$; ——, $\beta = 0.15$; —·—, $\beta = \infty$.

equation ($\beta = 0$) away from the Dirichlet frequencies, but it is substantially larger in their vicinity. In terms of the conditioning of the modified equation, this translates into a somewhat poorer conditioning relative to the Green equation away from the Dirichlet frequencies but a substantially better conditioning near these frequencies. Moreover, the modified equation with the optimal β enjoys a substantially better conditioning relative to the first-kind equation ($\beta = \infty$) both near and away from the Neumann frequencies. We may therefore conclude that introducing an optimal 11% of the first-kind component in the modified equation substantially improves the conditioning of the first-kind component alone over the entire frequency range and of the second-kind component alone (Green equation) near the Dirichlet frequencies,

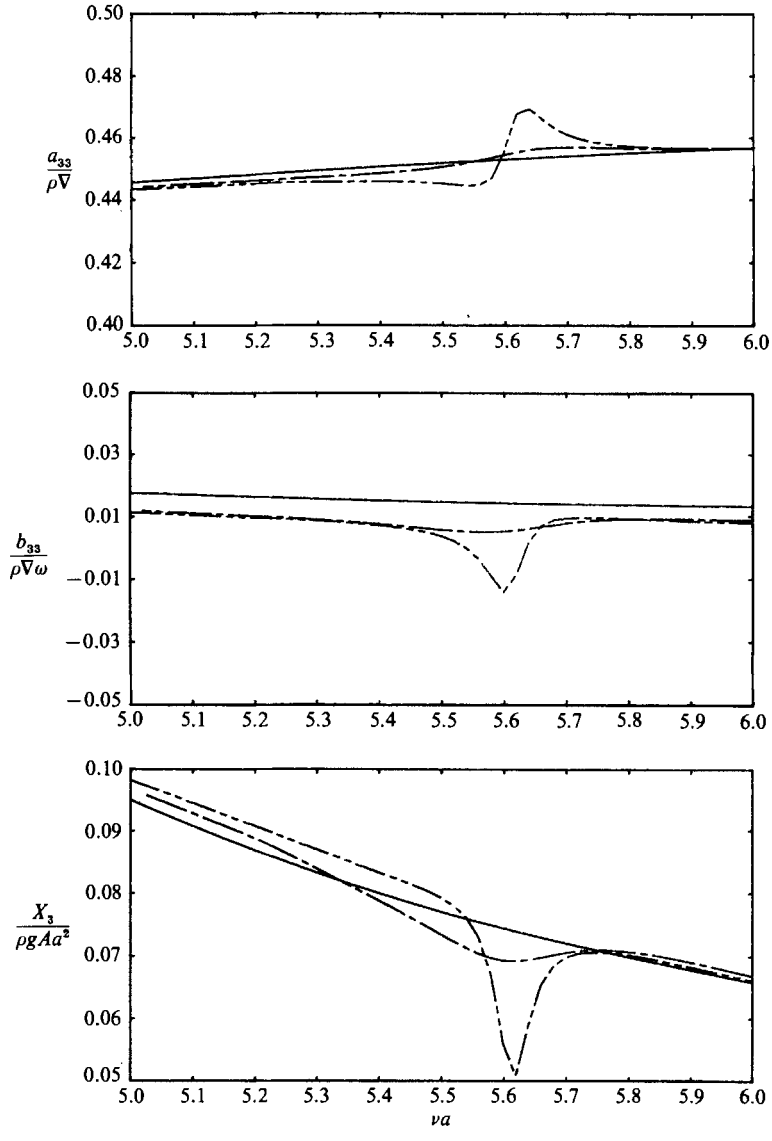

FIGURE 10. Heave added-mass and damping coefficients and modulus of the exciting force on the sphere near the second Dirichlet irregular frequency, as functions of νa: — — — —, $\beta = 0$; ——, $\beta = 0.11$; —·—, $\beta = \infty$.

while degrading somewhat the conditioning relative to the latter component away from these frequencies.

Our conclusions so far have been based on the premise that α is optimized at the first Dirichlet frequency. Numerical experimentation with the higher Dirichlet frequencies suggested similar if not somewhat inferior results. We did not attempt an optimization at the Neumann frequencies since the second-kind component is the dominant portion of the modified equation (4.1). Tests for the sphere and a truncated vertical cylinder suggested that β_{opt} is the same for all modes of oscillation of the same body but different for the two bodies. Finally, the approximate location of the first and higher Dirichlet frequencies was determined from the minima of λ for

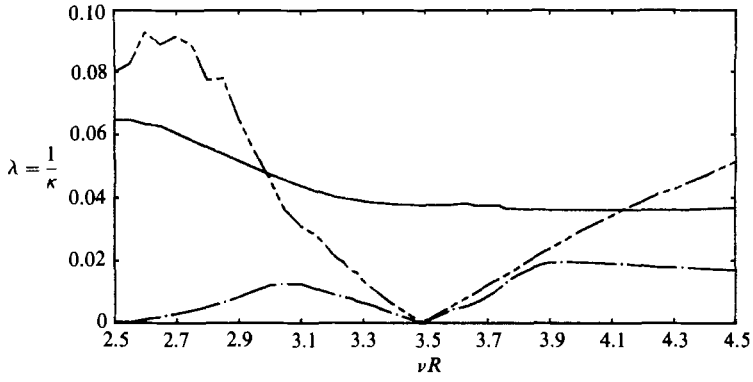

FIGURE 11. Inverse of the condition number λ near the common irregular frequency of equations (2.8) and (3.15) for the cylinder oscillating in heave, as functions of the non-dimensional wavenumber νR: — - - —, $\beta = 0$; ——, $\beta = 0.15$; —·—, $\beta = \infty$.

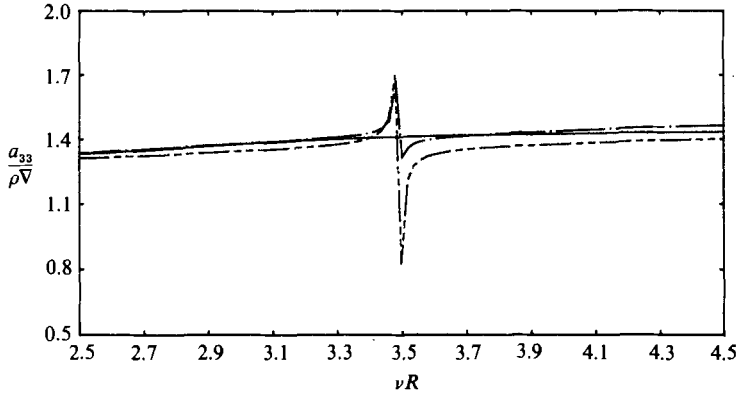

FIGURE 12. Heave added mass on the cylinder near the common irregular frequency of equations (2.8) and (3.15), as functions of νR: — - - —, $\beta = 0$; ——, $\beta = 0.15$; —·—, $\beta = \infty$.

the Green equation which locates their position with sufficient accuracy for the present analysis to be successful.

Figures 6 and 7 illustrate the performance of the method in predicting the sphere heave hydrodynamic coefficients and exciting-force modulus near the first Dirichlet and the first non-zero Neumann frequency respectively. The corresponding results for a truncated circular cylinder (draught/radius = 0.5) in the sway mode are shown in figures 8 and 9. For the cylinder, $\beta_{\text{opt}} = 0.15$. It may be observed in figure 7 that the performance of the first-kind equation ($\beta = \infty$) is quite inferior relative to both the Green equation or the optimal modified equation. The small discrepancy between the last two equations for the heave damping coefficient is due to its very small value which renders it unimportant in practice. Where the value of the damping coefficient is large, this discrepancy disappears as can be seen in the sway damping coefficient for the cylinder (figure 9).

Figures 6–9 illustrated the performance of the optimal modified equation in the vicinity of the first Dirichlet and second Neumann frequency for the heaving sphere and the first Dirichlet and first Neumann frequency for the swaying cylinder. A similar performance has been observed near the higher Dirichlet and Neumann

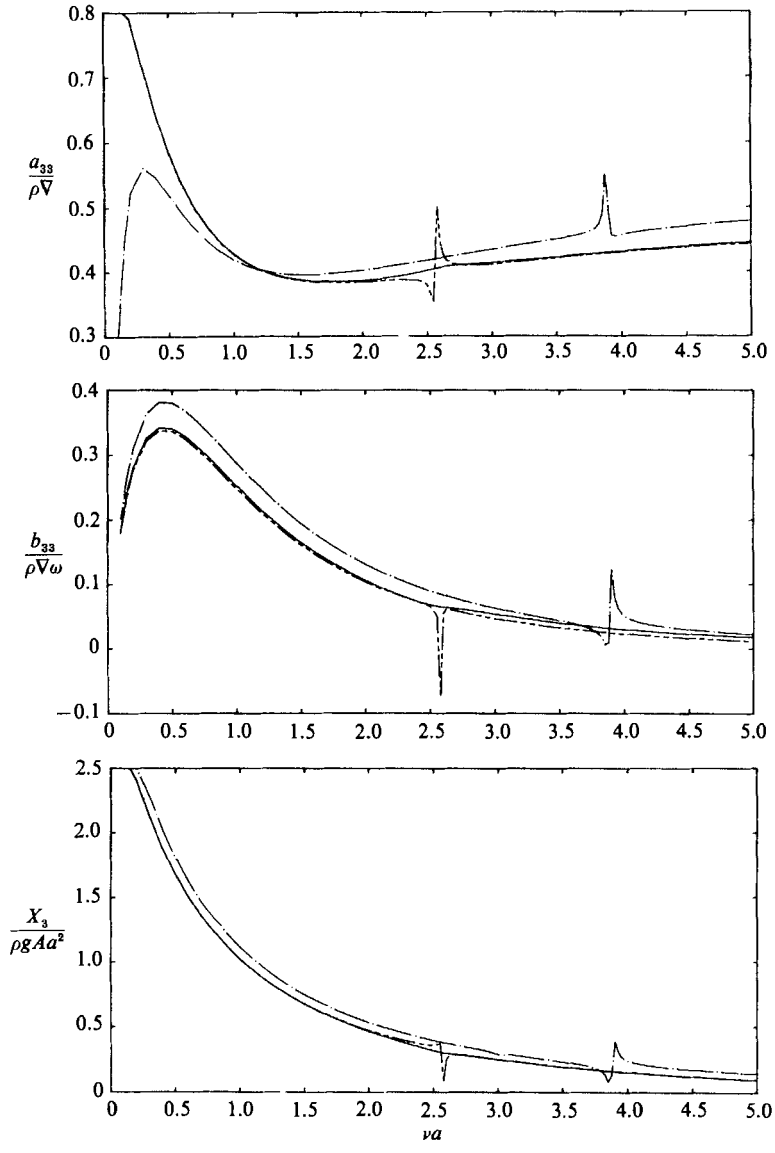

FIGURE 13. Heave added-mass and damping coefficients and modulus of the exciting force on the sphere, as functions of νa: — — —, $\beta = 0$; ——, $\beta = 0.11$; —·—, $\beta = \infty$.

frequencies, which typically lie at the border or outside the range of frequencies of interest in practice. The performance of the method near the second heave Dirichlet frequency of the sphere is illustrated in figure 10. The small discrepancy between the Green equation and the optimal modified equation for the damping coefficient away from that frequency is again because the evaluated quantity is very small. A similar performance has been observed near the higher Neumann frequencies. In all cases illustrated so far the entire surface of the sphere has been approximated with 256 panels and of the cylinder with 288 panels.

It was shown in §3 that for the truncated vertical cylinder the Dirichlet and Neumann frequencies may coalesce for specific values of the draught/radius parameter δ. For example, for $\delta = 0.367$ their coalescence occurs at the non-

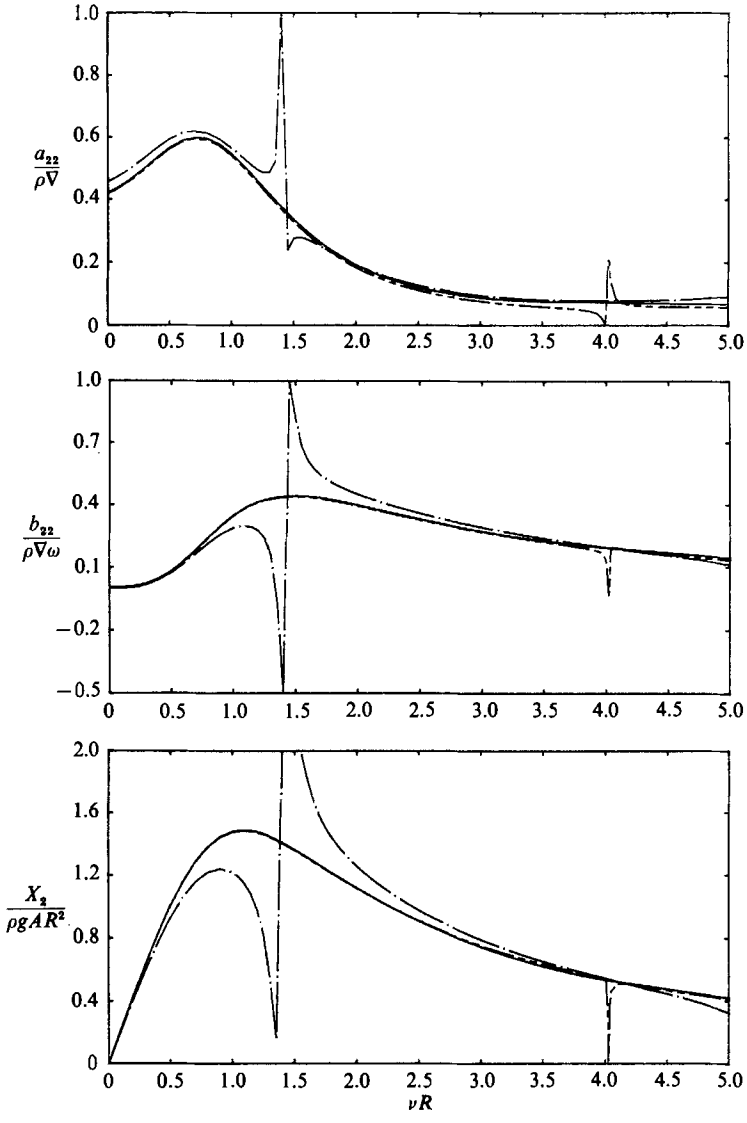

FIGURE 14. Sway added mass and damping coefficients and modulus of the exciting force on the cylinder, as functions of νR: – – – –, $\beta = 0$; ——, $\beta = 0.15$; —·—, $\beta = \infty$.

dimensional wavenumber $\nu R = 3.398$. The approximation of the surface of a cylinder with 288 panels for this value of δ revealed that the zeros of λ for the first- and second-kind equations separately did not exactly coalesce. This is due to a 'numerical shift' of the corresponding frequencies caused by the approximation of the surface of the cylinder with a finite number of panels. Numerical experimentation with $N = 288$ panels led to a coalescence of the zeros of the corresponding λ values for $\delta = 0.352$ at $\nu R = 3.5$. This is illustrated in figure 11 which shows the variation of λ for the Green equation ($\beta = 0$), the first-kind equation ($\beta = \infty$) and the modified equation with $\beta = 0.15$. The non-vanishing value of λ for the modified equation confirms the absence of ill-conditioning, shown analytically in §3. The performance of the three equations in predicting the heave added-mass coefficient is illustrated in figure 12.

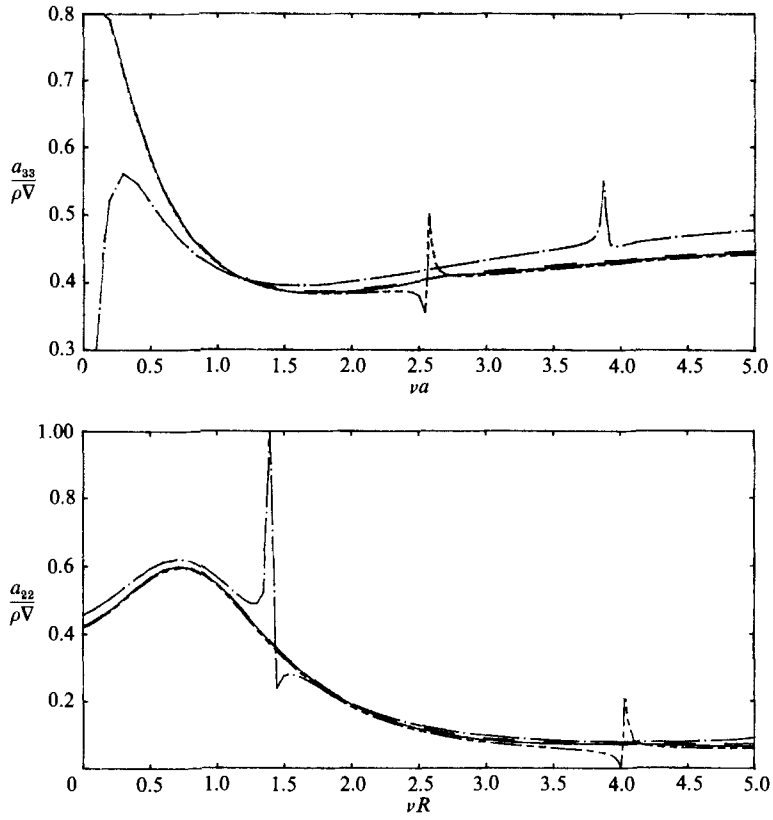

FIGURE 15. Heave added mass of the sphere and sway added mass of the cylinder, as functions of νa and νR: — — — —, $\beta = 0$; — —, β_{opt}; ——, $\beta = 0.2$; — · —, $\beta = \infty$.

All results presented so far studied the performance of the second-kind, first-kind and modified equations near the Dirichlet and Neumann frequencies. Their performance over a wide frequency range for the heaving sphere and the swaying cylinder is illustrated in figures 13 and 14 respectively. The following observations can be made: (i) as expected, the spiky error in the first-kind equation occurs at the Neumann frequencies and in the second-kind equation at the Dirichlet frequencies; (ii) away from the Neumann frequencies, the performance of the first-kind equation is poor in comparison to the second-kind and the modified equations due to its substantially poorer conditioning; (iii) the agreement between the second-kind and the modified equation is very good away from the Dirichlet frequencies, and the performance of the latter much better in their vicinity; (iv) small discrepancies between the second-kind and the modified equations are observed only where the evaluated quantity is small in value, their agreement being very satisfactory when this value is large. Therefore, the performance of the modified equation is very satisfactory away from the Dirichlet frequencies, indicating that its poorer conditioning than the Green equation there (see figure 5) does not translate into appreciable errors.

The determination of β_{opt} for the specific geometry being studied requires the determination of the first Dirichlet frequency, followed by the maximization of the λ-parameter by varying β. In practice, this process may be responsible for a

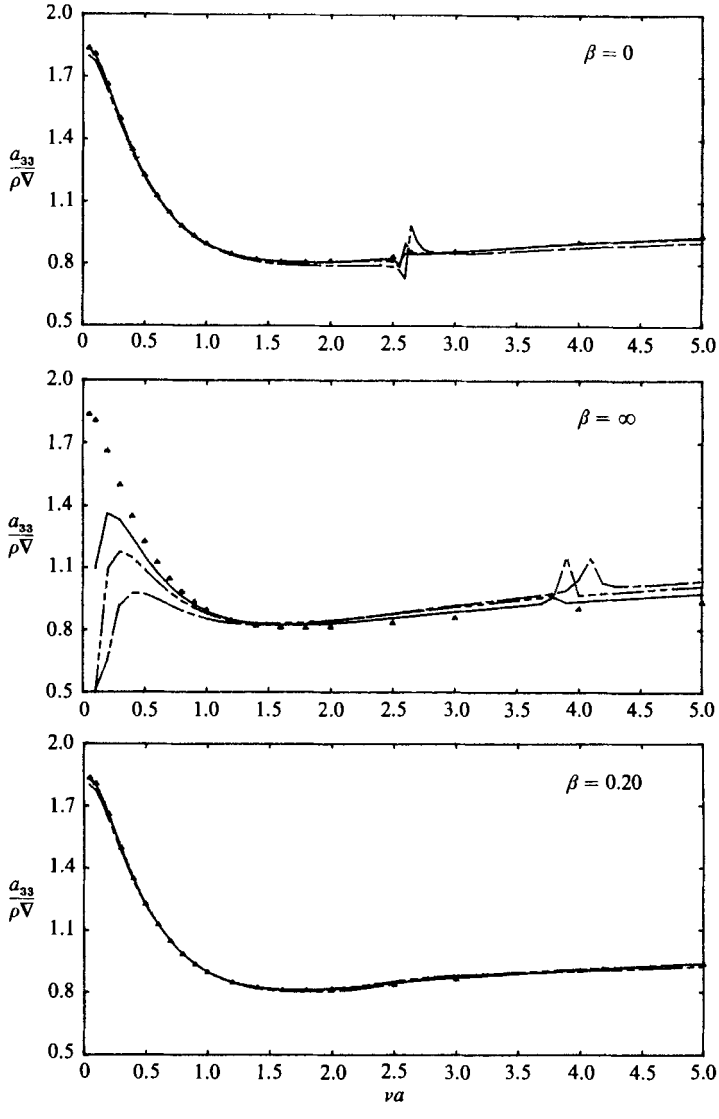

FIGURE 16. Heave added masses of a sphere computed with three discretizations are compared with Hulme (▲): — — —, 64 panels; — — — —, 256; ——, 1024.

substantial computational overhead. For all the bodies studied, the optimal value of β is less than 0.2. Furthermore, it may be seen from figures 3 and 4 that the decay of λ for values of β greater than β_{opt} is gradual. Therefore, selecting a value for β in (4.1) that would be an upper bound of the optimal values for a range of bodies of practical interest may not substantially degrade the quality of the predicted hydrodynamic forces. The value $\beta = 0.2$ was selected and has been used in figure 15 for the evaluation of the heave added mass of the sphere and the sway added mass for the cylinder, generating good results over a wide frequency range.

The convergence of the solution of the modified integral equation has been tested for three different values of β: 0, 0.2 and ∞. Here, we used flat panels and piecewise-constant values for the potential on each panel. As an example, the added-mass and

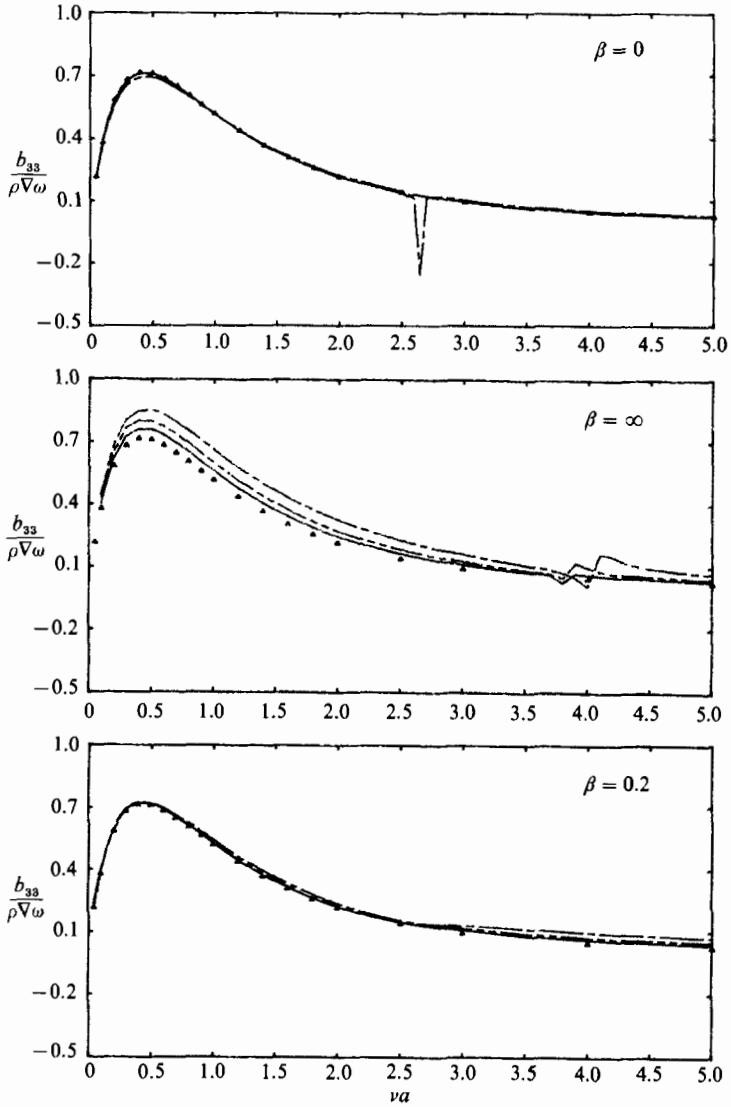

FIGURE 17. Heave damping coefficients of a sphere computed with three discretizations are compared with Hulme (▲): — — —, 64 panels; — — — —, 256; ——, 1024.

damping coefficient of a sphere are computed in heave and surge for three discretizations (64, 256 and 1024 panels) and compared to the highly accurate results of Hulme (1983) in figures 16–19. From these figures we observe that the first-kind equation does converge to the correct solution even though the convergence rate is much slower than that of the second kind. We can attribute the slower convergence of the first-kind equation to two sources: its poorer conditioning, and the wider bandwidth of the Neumann irregular frequency compared to that of the Dirichlet irregular frequency. The first source influences the entire frequency range while the second source influences the convergence only in the vicinity of the Neumann frequencies. The slower convergence of the first-kind equation is strongly influenced by the second source as is illustrated in the figures 16, 18 and 19 where the solution converges fairly fast except near the Neumann frequencies (the zero frequency is the

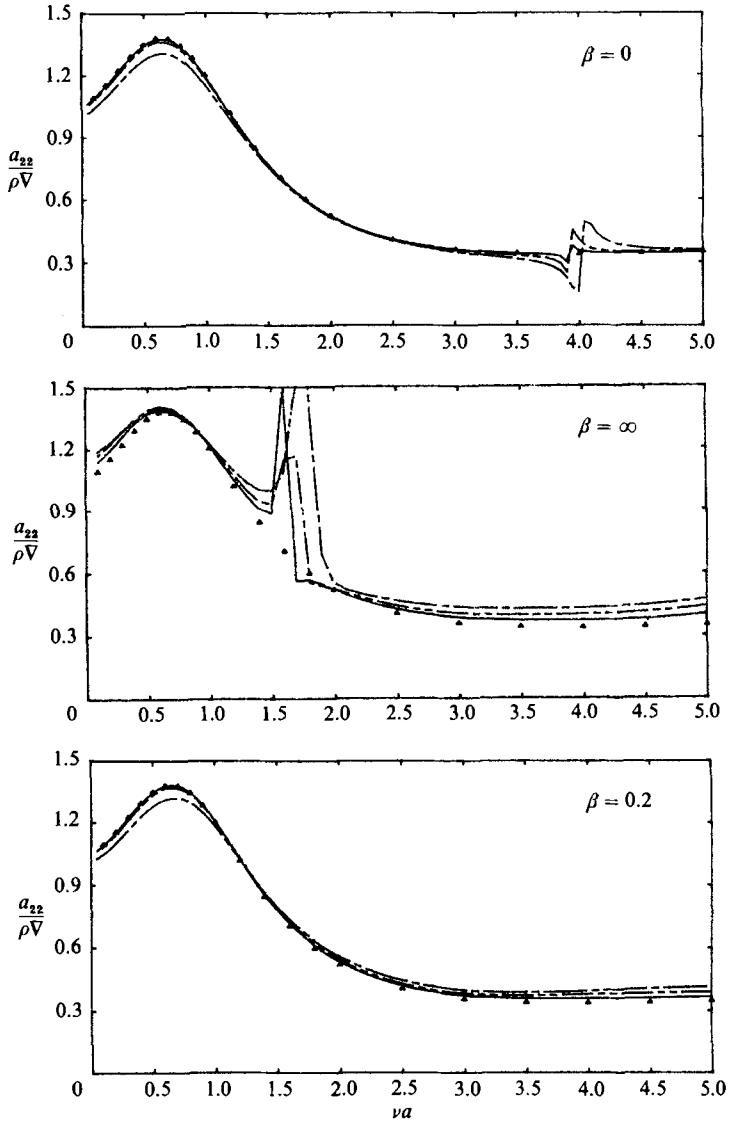

FIGURE 18. Surge added masses of a sphere computed with three discretizations are compared with Hulme (▲): — — —, 64 panels; — — — —, 256; ——, 1024.

first Neumann frequency for the heave mode). Finally, the convergence of the modified integral equation for $\beta = 0.2$ is a little slower than those of second-kind but much faster than that of the first-kind throughout the frequency range computed. From above, we may conclude that the solution of the modified integral equation converges to the correct solution with convergence rate which depends on the value of β, and that the modified integral equation with the optimum β shows good convergence which is confirmed by the very good agreement of the computed hydrodynamic coefficient with the result of Hulme (1983).

Relative to the Green equation ($\beta = 0$), the additional computational effort for the set-up and solution of (4.1) requires the evaluation of the influence coefficients which involve the double normal derivative of the Green function. The corresponding influence coefficients in the right-hand side involve single derivatives of G which are

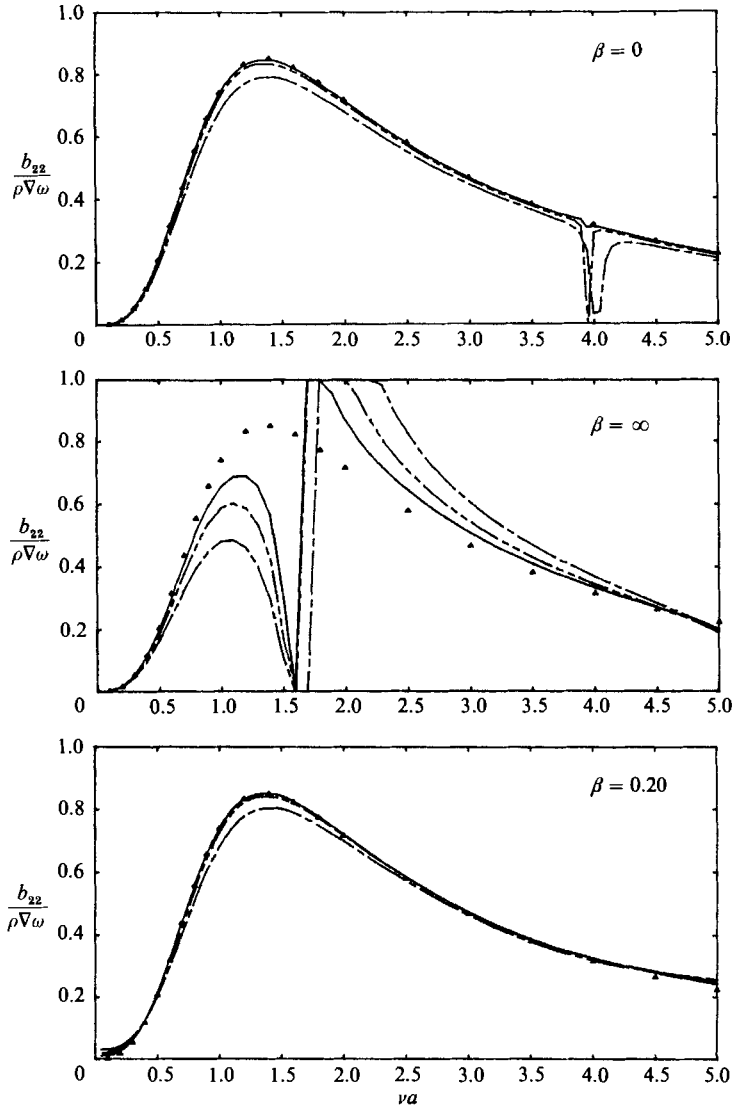

FIGURE 19. Surge damping coefficients of a sphere computed with three discretizations are compared with Hulme (▲): — — —, 64 panels; — — — —, 256; ——, 1024.

evaluated for the set-up of the Green equation. In deep water, the second spatial derivatives of G are related to its single derivatives and values by simple recurrence relations (Newman 1985) which require a few floating-point operations for their implementation. In finite water depth such recurrence relations are not known. It is, however, possible to develop algorithms for the evaluation of the Green function that may not require a substantial effort for the evaluation of the double derivatives relative to that required for their single derivatives and values. The solution of the linear system requires the same effort as for the Green equation, since the total number of panels is the same. In deep water, it has been our experience for the sphere and the cylinder that the increase in the computational effort relative to the solution of the Green equation is about 20%. If the recommended value $\beta = 0.2$ for the coupling does not perform well for a particular geometry a new optimal value of β

must be determined. This is accomplished by estimating the position of the irregular frequency followed by the determination of the minimum condition number over a range of values of β. This search would in principle involve a substantial increase in the computational effort relative to cases where the value of β is set *a priori*.

The effects and importance of irregular frequency on multi-component structures and in particular on Tension Leg Platforms are further discussed by Korsmeyer *et al.* (1988). A more extensive presentation and additional results from the present method can be found in Lee (1988).

5. Conclusions

A modified integral equation has been studied for the removal of all the irregular frequencies from boundary-integral equations arising in three-dimensional wave–body interactions. It has been obtained by the linear combination of the Green equation and its normal derivative relative to the field point, multiplying the latter by a complex coupling constant. The unbounded operator resulting from taking the normal derivative of the Green equation has not been regularized as has been suggested in the acoustics literature. Instead it has been directly discretized, using a panel code which employs plane quadrilateral panels to approximate the body boundary, a piecewise-constant variation of the velocity potential and point collocation at the panel centroids.

The effectiveness of the method depends on the proper selection of the coupling constant. It was numerically shown by minimizing the condition number of the modified equation at the first irregular frequency of the Green equation, that an optimal phase, equal to 90°, and modulus exist. The value of the optimal modulus was found to depend on the shape of the body geometry, but a value of 0.2 was found to generate satisfactory results for the bodies tested. The implementation of the method does not entail a substantial increase in computational effort relative to the solution of the Green equation since the number of panels is the same, and in deep water the double spatial derivatives of the Green function can be expressed in terms of its first spatial derivatives and values by simple recurrence relations. The performance of the method has been demonstrated by evaluating the added-mass and damping coefficients and exciting force on a sphere and a truncated vertical cylinder.

Financial support for this study was provided by A. S. Veritec, and by the Office of Naval Research (Contract N0014-8222-K-0198).

REFERENCES

ADACHI, H. & OHMATSU, S. 1979 On the influence of irregular frequencies in the time-dependent free surface problems. *J. Soc. Nav. Arch. Japan* **146**, 119–128.

ANGELL, T. S., HSIAO, G. C. & KLEINMAN, R. E. 1986 An integral equation for the floating body problem. *J. Fluid Mech.* **166**, 161–171.

BAI, K. J. & YEUNG, R. W. 1974 Numerical solutions to free-surface flow problems. In *Proc. 10th Symp. Nav. Hydrodyn., Cambridge, MA*, pp. 609–633.

BRAKHAGE, H. & WERNER, P. 1965 Uber das Dirichletsche Aussenraumproblem fur die Helmholtzsche Schwingungsgleichung. *Arch. Math.* **16**, 325–329.

BREIT, S. R., NEWMAN, J. N. & SCLAVOUNOS, P. D. 1985 A new generation of panel programs for radiation-diffraction problems. *Proc. BOSS'85 Conf., Delft.*

BURTON, A. J. & MILLER, G. F. 1971 The application of integral equation methods to the numerical solution of some exterior boundary-value problems. *Proc. R. Soc. Lond.* A **323**, 201–220.

COLTON, D. & KRESS, R. 1983 *Integral Equation Methods in Scattering Theory*. Wiley Interscience.

EUVRARD, D., JAMI, A., LENOIR, M. & MARTIN, D. 1981 Recent progress towards an optimal coupling of finite elements and singularity distribution procedures in numerical ship hydrodynamics. *Proc. 3rd Intl Conf. Num. Ship Hydrodyn, Paris.*

FRANK, W. 1967 Oscillation of cylinders in or below the free surface of deep fluids. *Rep.* 2375. Naval Ship Res. and Dev. Center, Bethesda, MD.

HESS, J. L. & SMITH, A. M. O. 1966 Calculation of non-lifting potential flow about arbitrary bodies. *Prog. Aero. Sci.* **8**, 1–138.

HSIAO, G. C. & KRESS, R. 1985 On an integral equation for the two-dimensional exterior Stokes problem. *Appl. Numer. Maths* **1**, 77–93.

HULME, A. 1983 A ring-source/integral-equation method for the calculation of hydrodynamic forces exerted on floating bodies of revolution. *J. Fluid Mech.* **128**, 387–412.

JOHN, F. 1950 On the motion of floating bodies. II. Simple harmonic motions. *Communs Pure Appl. Maths* **3**, 45–101.

KELLOG, O. D. 1929 *Foundations of Potential Theory*. Springer.

KLEINMAN, R. E. 1982 On the mathematical theory of the motion of floating bodies – an update. *DTNSRDC Rep.* 82/074.

KORSMEYER, F. T., LEE, C.-H., NEWMAN, J. N. & SCLAVOUNOS, P. D. 1988 The analysis of wave effects on tension-leg platforms. *OMAE Conf., Houston.*

KRESS, R. 1983 Minimizing the condition number of boundary integral operators in acoustic and electromagnetic scattering. *NAM-Bericht Nr.* 35, pp. 1–30.

LEE, C.-H. 1988 Numerical methods for the solution of three-dimensional integral equations in wave–body interactions. Ph.D. thesis, Department of Ocean Engineering, MIT.

LEIS, R. 1965 Zur Dirichletschen Randwertaufgabe des Aussenraums der Schwingungsgleichung. *Math. Z.* **90**, 205–211.

MARTIN, P. A. 1981 On the null-field equations for water-wave radiation problems. *J. Fluid Mech.* **113**, 315–332.

MEI, C. C. 1978 Numerical methods in water-waves diffraction and radiation. *Ann. Rev. Fluid Mech.* **11**, 289–316.

MORAN, J. 1984 *An Introduction to Theoretical and Computational Aerodynamics*. Wiley.

NESTEGARD, A. & SCLAVOUNOS, P. D. 1984 A numerical solution of two-dimensional deep water wave–body problems. *J. Ship Res.* **28**, 48–54.

NEWMAN, J. N. 1985 Algorithms for the free-surface Green functions. *J. Engng Maths.* **19**, 57–67.

NEWMAN, J. N. 1986 Distributions of sources and normal dipoles over a quadrilateral panel. *J. Engng Maths* **20**, 113–126.

OGILVIE, T. F. & SHIN, Y. S. 1978 Integral-equation solutions for time-dependent free-surface problems. *J. Soc. Nav. Arch. Japan* **143**, 86–96.

OHMATSU, S. 1975 On the irregular frequencies in the theory of oscillating bodies. *Papers, Ship Res. Inst.*, No. 48.

PANICH, O. I. 1965 On the question of the solvability of the exterior boundary-value problems for the wave equation and Maxwell's equations. *Russ. Math. Surv.* **20**, 221–226.

SAYER, P. 1980 An integral-equation method for determining the fluid motion due to a cylinder heaving on water of finite depth. *Proc. R. Soc. Lond.* A **372**, 93–110.

SCLAVOUNOS, P. D. & LEE, C. H. 1985 Topics on boundary-element solutions of wave radiation-diffraction problems. In *Proc. 4th Intl Conf. Num. Ship Hydrodyn., Washington.*

URSELL, F. 1981 Irregular frequencies and the motions of floating bodies. *J. Fluid Mech.* **105**, 143–156.

WEHAUSEN, J. V. & LAITONE, E. V. 1960 *Surface Waves*. Handbuch der Physik, Vol. 9, pp. 446–778, Springer.

WU, X. J. & PRICE, W. G. 1987 A multiple Green's function expression for the hydrodynamic analysis of multi-hull structures. *Appl. Ocean Res.* **9**, 58–66.

YEUNG, R. W. 1973 A singularity-distribution method for free-surface flow problems with an oscillating body. *Rep.* NA 73-6, College of Engng, Univ. of Cal., Berkeley.